Solid State Ionics 269 (2015) 24–29

Contents lists available at ScienceDirect

Solid State Ionics

journal homepage: www.elsevier.com/locate/ssi

Characterization of $LaNi_{0.6}Fe_{0.4}O_3$ perovskite synthesized by glycine-nitrate combustion method

K. Vidal [a,*], A. Morán-Ruiz [a], A. Larrañaga [a], J.M. Porras-Vázquez [b], P.R. Slater [b], M.I. Arriortua [a,*]

[a] Universidad del País Vasco/Euskal Herriko Unibertsitatea (UPV/EHU), Dpto. Mineralogía y Petrología, Apdo. 644, E-48080 Bilbao, Spain
[b] University of Birmingham, School of Chemistry, Birmingham B15 2TT, UK

ARTICLE INFO

Article history:
Received 8 May 2014
Received in revised form 27 October 2014
Accepted 3 November 2014
Available online 26 November 2014

Keywords:
Chemical synthesis
Electrical conductivity
Contact material
Perovskite phases
SOFC

ABSTRACT

The perovskite $LaNi_{0.6}Fe_{0.4}O_3$ has been prepared by the glycine–nitrate route using different amounts of glycine/fuel ratio (G/N = 0.5, 1.0 and 1.5), in order to study the sample preparation influence on the properties in the context of their application as a cathode contact material for solid oxide fuel cells (SOFCs). The obtained materials have been characterized by X-ray diffraction, scanning electron microscopy, dilatometry and electrical conductivity measurements. All the compounds have rhombohedral symmetry and a porous microstructure with fine grain sizes. The sample obtained at the G/N of 1.0 has more suitable conductivity values for application as SOFC contact material.

1. Introduction

The need for a clean and efficient energy conversion is a critical technological and economic challenge. Solid oxide fuel cells (SOFCs) have a substantial potential in the application of a clean and efficient electrical power generation. However, the widespread utilization of SOFCs has not been realized because the cost associated with cell fabrication, materials and maintenance is still too high [1].

The development of new materials, as well as advanced SOFC component fabrication techniques, is critical in reducing operation temperature and subsequently in lessening the cost of these systems. Traditionally, most of these ceramic materials have been prepared from the mixture of their constituent oxides in the so called solid state reaction, "shake and bake" or ceramic method, a preparative route which presents as a fundamental handicap the necessity of heating the precursors at high temperature for large periods of reaction time to reach the formation of a desired phase. Therefore, the use of such drastic experimental conditions drives the formation of materials that show particles with a relatively large size [2]. Alternative routes to the solid state reaction method are wet chemical synthetic methods such as co-precipitation (with oxalates, carbonates, cyanides or any other salt precursors), combustion (including all variants from low to high temperature), sol–gel (and all of its modifications with different chelating ligands), spray-pyrolysis, and metathesis reactions. In all cases the idea is to accelerate the pure phase formation, a goal that is achieved due to the liquid media which permit the mixing of the elements at the atomic level, thus resulting in lower firing temperatures [3,4]. Other advantages of these methods are the possibility of having a controlled particle size, morphology and improvement in surface area. Particularly, combustion methods have been proposed as one of the most promising methods to prepare perovskite oxide powders to be used as electrode materials in solid oxide fuel cell technology [5].

Combustion reaction is one of the most accessible, fast and low energy soft methods for the synthesis of a variety of advanced ceramics, catalysts and nanomaterials [6,5]. Combustion synthesis (CS) methods can be classified into three categories, on the basis of the physical nature of reaction mixture itself: (i) flame synthesis or gas phase combustion, (ii) heterogeneous condensed phase combustion synthesis and (iii) solution combustion synthesis (SCS) [6,7]. Focusing our attention on the SCS route, it involves a self-sustained exothermic reaction between an oxidizer (e.g. metal nitrate) and a fuel (e.g. urea, glycine, hydrazides, carbohydrazide). Compared with the ceramic method this synthetic route has much faster reaction times and lower calcination temperatures leading to powders with large compositional homogeneity and nanometric particle sizes, which are desired characteristics for this type of applications. The characteristics (including the purity, structure and size) of the combustion synthesis oxide powders are typically determined by several synthetic parameters, such as the species of fuel and oxidizer reactants, the fuel/oxidizer ratio, and the subsequent sintering treatment after combustion process [8]. The fuel to oxidizer ratio is considered to be the most important one in varying the final properties [9]. This parameter may influence the phase formation

* Corresponding authors. Tel.: +34 946015984; fax: +34 946013500.
E-mail addresses: karmele.vidal@ehu.es (K. Vidal), maribel.arriortua@ehu.es (M.I. Arriortua).

http://dx.doi.org/10.1016/j.ssi.2014.11.002
0167-2738/

process [10], the phase structure of the products [11], the morphology of the as-prepared powders [12], and then, the physical and chemical properties of the materials [13].

Earlier studies have concluded that the use of cathode contact layers improves electron transfer through the contact interface from the interconnect to the cathode layer [14,15]. The cathode contact material composition is required to possess high electrical conductivity and appropriate sintering activity to minimize the resistance of the contact layer itself and to protect the steel substrate from excessive oxidation. Besides, it should demonstrate an appropriate thermal expansion behavior and high thermochemical and structural stability in the oxidizing cathode environment [16,17].

In this study $LaNi_{0.6}Fe_{0.4}O_3$ is selected for its use as contact layers, due to the adequate sintering activity, electrical conductivity, thermal expansion coefficient (TEC), integrity and low reactivity between the interconnect and cathode without compromising the contact resistance of the system [14,18].

Continuing our research on $La(Ni,Fe)O_3$ based systems, in the present work we investigate the effect of the variation of the fuel/oxidizer ratio of glycine/nitrate (G/N = 0.5, 1.0 and 1.5) on the structural, morphological and electrical properties of the $LaNi_{0.6}Fe_{0.4}O_3$ perovskite oxide.

2. Experimental

2.1. Powder preparation

The compound $LaNi_{0.6}Fe_{0.4}O_3$ was prepared by the glycine-nitrate method starting from the reagents $La(NO_3)_3 \cdot 6H_2O$ (>99%), $Ni(NO_3)_2 \cdot 6H_2O$ (98.5%) and $Fe(NO_3)_2 \cdot 9H_2O$ (98.5%), all from Aldrich. These metal nitrates were dissolved in distilled water. The solutions were mixed in a 1 l glass beaker, which was put on a hot plate, under constant stirring, to evaporate excess water. For examining the effect of combustion fuel condition on the properties of the final powder, different combustion fuel conditions were designed by adding different amounts of fuel. Then, the glycine was added to obtain a glycine/nitrate molar ratio of 0.5, 1.0 and 1.5, respectively. The resulting viscous liquid autoignited after putting the glass beaker directly in a preheated plate (at 450 °C). The resulting powders were pelletized and calcined in air at 850 °C for 6 h to obtain the pure sample.

2.2. Characterization techniques

Room temperature X-ray powder diffraction (XRD) data were collected in the $18 < 2\theta < 110°$ range with an integration time of 10 s/0.02° step using a Philips X'Pert-PRO X-ray diffractometer with secondary beam graphite monochromated Cu–Kα radiation. All samples were single phase without detectable impurities. The crystal structure was refined by the Rietveld method [19] using the GSAS software package [20].

Compositional analysis was performed on all prepared samples to confirm that the expected elemental composition was achieved. All metal contents were determined by inductively coupled plasma atomic emission spectroscopy (ICP-AES) on a Horiba Yobin Yvon Activa spectrophotometer.

The morphologies of the powder samples and of the sintered pellets were observed using a scanning electron microscope (JEOL JSM-7000F). Secondary electron images were taken at 20 kV and $1.1.10^{-11}$ A using a working distance of 8 mm.

For bulk conductivity and thermal expansion (TEC) measurements, pellets of powders were sintered at 1050 °C, and then, cut in $1 \times 3 \times 7$ mm bars. The bulk density of each sample was calculated by measuring the mass and the dimensions of the bars. The samples had a density of around 75% of the theoretical (X-ray) density. DC conductivity measurements were performed in air by the four-point DC method (Thurlby Thandar Instruments 1604 digital multimeter and Thurlby Thandar Instruments PL300 current source). Electrical contacts were made using Pt wires and Pt paste placed over whole end faces ensuring a homogeneous current flow. Voltage contacts were made as small as possible to avoid any disturbance of the contacts on the current flow. Measurements were performed from 300 °C to 850 °C. The conductivity (σ) was determined from a set of V–I values by taking $\sigma = 1 / \rho = L / A \times dI / dV$, where L is the distance between voltage contacts and A is the sample cross section. Finally, TEC measurements were carried out from room temperature to 1000 °C in air with a heating rate of 5 °C/min by using a Unitherm Model dilatometer.

3. Results and discussion

3.1. Structural study

Fig. 1 shows the remarkable dependence of phase constitution on fuel condition for the combustion products depending on the glycine/nitrate molar ratio. In the case of the $LaNi_{0.6}Fe_{0.4}O_3$ sample with stoichiometric G/N, the combustion synthesis produced a clearer and brighter flame, and a higher reaction temperature, in comparison with both the samples obtained under an oxidizer and fuel rich conditions, respectively. According to this, as can be observed in the figure, for the sample prepared using a glycine/nitrate molar ratio of 1.0, the product obtained from combustion (as synthesized powders without applying caltination temperature of 850 °C), is nearly a single phase and is better crystallized compared with the other two compounds.

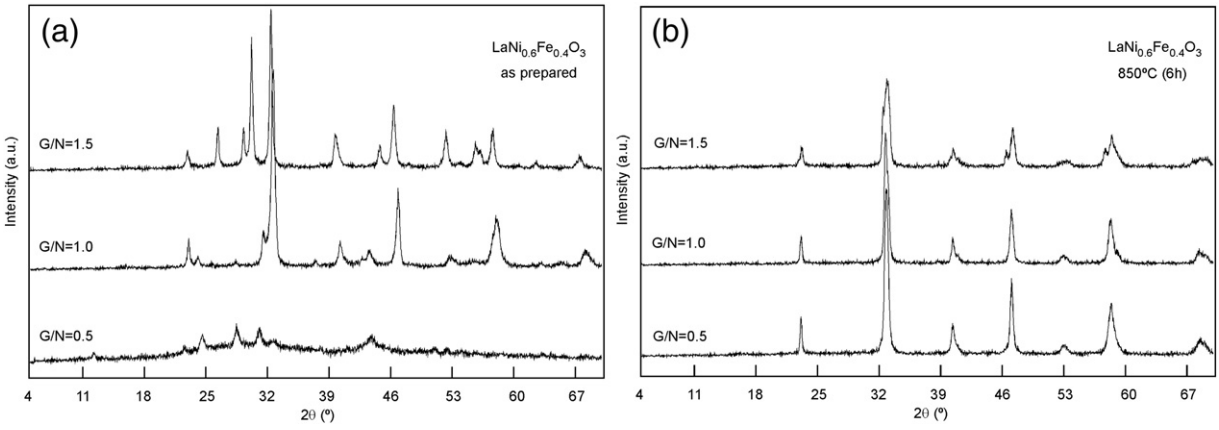

Fig. 1. X-ray diffraction patterns measured (a) before and (b) after calcination at 850 °C for $LaNi_{0.6}Fe_{0.4}O_3$ perovskites obtained by the glycine-nitrate route using different amounts of fuel/oxidizer ratio (G / N = 0.5, 1.0 and 1.5), respectively.

Table 1
Summary of the ICP analyses.

G/N	Nominal composition	Experimental composition
0.5	$LaNi_{0.6}Fe_{0.4}O_3$	$La_{0.96(2)}Ni_{0.61(1)}Fe_{0.40(1)}O_3$
1.0	$LaNi_{0.6}Fe_{0.4}O_3$	$La_{1.00(2)}Ni_{0.63(2)}Fe_{0.40(1)}O_3$
1.5	$LaNi_{0.6}Fe_{0.4}O_3$	$La_{0.98(2)}Ni_{0.63(1)}Fe_{0.41(1)}O_3$

Nevertheless, as shown by the X-ray diffraction patterns, the three $LaNi_{0.6}Fe_{0.4}O_3$ samples were obtained without impurities by applying a calcination temperature of 850 °C in air during 6 h after combustion synthesis.

Results from chemical analyses are presented in Table 1, showing a good agreement between the analyzed chemical compositions of the prepared powders and the nominal compositions.

Fig. 2 shows the Rietveld refinement of the XRD data for the $LaNi_{0.6}Fe_{0.4}O_3$ samples obtained after applying a calcination temperature of 850 °C. The analysis of the X-ray diffraction (XRD) data indicated

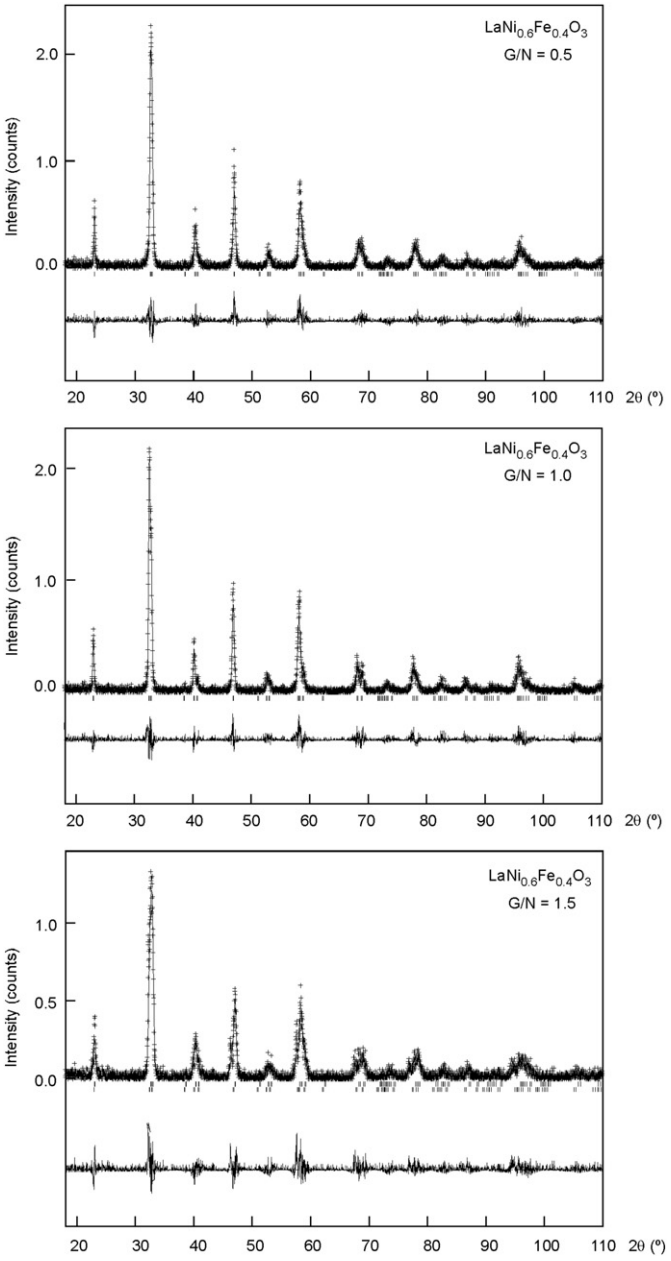

Fig. 2. Rietveld fits of the XRD data for the samples using rhombohedral R$\bar{3}$c space group.

that the samples with G/N = 0.5 and 1.0 crystallized as a single phase in the rhombohedral space group R$\bar{3}$c. For the compound with G/N 1.5, however, the appearance of extra shoulders in the experimental profile indicates a possible phase segregation to give two perovskite phases of different Ni/Fe ratio. The introduction of two R$\bar{3}$c phases improves satisfactorily the profile fitting of this sample.

Final refined values of the structural parameters are summarized in Table 2. A slight decrease in lattice parameters and cell volume is observed with increasing G/N molar ratio. These obtained values are in good agreement with reported parameters [14,21–23].

As can be seen, the average La–O, (Ni,Fe)–O and La–(Ni,Fe) bond distances vary slowly with a small reduction of the (Ni,Fe)–O–(Ni,Fe) angles with the increase of the G/N molar ratio. According to other works [5], by increasing the fuel/oxidant ratio, the perovskite structure changes to a less symmetric structure. In this case, the variation observed seems to be due to a small change in mean ionic radius of the B site ions (Fe^{3+} and Ni^{3+}) as G/N ratio increases, due to varying degrees of oxygen vacancies and hence mean transition metal oxidation state.

3.2. Morphological study

Bevilacqua et al. [24], showed, for this composition, that the synthetic route has a strong influence on the sinterability of the final bars, indicating a different behavior of the materials during the sintering process at high temperatures. In addition, for a particular synthesis method, the experimental conditions used also play an important role in the properties of the final product. In this sense, it is well known that the fuel/oxidizer ratio may have some effects on the power sinterability, and then, on the overall electrical properties of the electrolyte and electrode materials [5,8].

Fig. 3 shows the well-necked morphology of the $LaNi_{0.6}Fe_{0.4}O_3$ powders synthesized by the combustion method and calcined at 850 °C, which are composed of nanosized particles and agglomerations of grains. These agglomerates formed during combustion reaction are usually soft and easy to break due to the higher volume of escaping gases for these samples [8,10].

The SEM micrographs taken on the surface of the three samples sintered (1050 °C during 5 h) bars are shown in Fig. 4.

The samples sintered at 1050 °C show particles of grain sizes of about 0.3–0.4 μm. The material with stoichiometric G/N value seems to sinter more easily with respect to the other two materials. Usually, a smaller particle size is beneficial to sintering and results in higher density when the sintering process is complete.

As previously mentioned, for the sample with G/N = 1.0, the observed flame was clear and bright, with a high ignition temperature (lower adiabatic flame temperature), which gives rise to the formation of less agglomerates, and then, to an increase in sinterability. However, regardless of the synthesis conditions, the porosity will decrease with increasing sintering temperature. Consequently, in this work, the low sintering temperature used may be a reason why the density values obtained for the rectangular bars are low [25].

3.3. Electrical conductivity study

Fig. 5 shows the relation between log(σT) versus the inverse absolute temperature. The electronic conductivity of $LaNi_xFe_{1-x}O_3$ series with $x \leq 0.6$, can be described by the thermally activated small polaron mechanism [24,26] which is generally expressed as:

$$\sigma = \frac{A}{T} \cdot \exp\left(-\frac{E_a}{kT}\right) \quad (1)$$

in which E_a is the activation energy for small polaron hopping conduction, k is the Boltzmann constant, T is the absolute temperature and A is a pre-exponential factor. Before making comparisons between the

Table 2
Structural parameters obtained by Rietveld refinement.

G/N	0.5	1.0	1.5 Rhombohedral	
Symmetry	Rhombohedral	Rhombohedral		
Space group	$R\bar{3}c$	$R\bar{3}c$	$R\bar{3}c$ (wt. frac. = 0.59)	$R\bar{3}c$ (wt. frac. = 0.41)
a (Å)	5.508 (1)	5.507 (1)	5.529 (2)	5.491 (2)
c (Å)	13.335 (2)	13.298 (2)	13.280 (3)	13.265 (2)
V / Z (Å^3)	350.3 (1)	349.2 (1)	351.6 (3)	346.4 (2)
$\rho_{the.}$ (g/cm^3)[a]	6.952	6.974	6.927	7.032
$Uiso_{(La)}$	1.12 (2)	1.52 (1)	1.60 (4)	2.70 (4)
$Uiso_{(Ni,Fe)}$	1.62 (2)	0.58 (1)	2.12 (4)	2.75 (4)
O x	0.467 (4)	0.453 (3)	0.451 (4)	0.447 (4)
$Uiso_{(O)}$	2.12 (2)	1.95 (2)	2.44 (4)	2.54 (4)
La–(Ni,Fe) (x2) (Å)	3.334 (1)	3.325 (1)	3.320 (1)	3.316 (1)
La–(Ni,Fe) (x6) (Å)	3.368 (1)	3.367 (1)	3.379 (1)	3.357 (1)
<La–(Ni,Fe)> (Å)	3.360 (1)	3.356 (1)	3.364 (1)	3.347 (1)
La–O (x3) (Å)	2.936 (2)	3.012 (2)	3.040 (3)	3.040 (3)
La–O (x3) (Å)	2.572 (2)	2.495 (2)	2.490 (3)	2.450 (3)
La–O (x6) (Å)	2.739 (1)	2.740 (1)	2.742 (3)	2.736 (3)
<La–O>	2.746 (1)	2.747 (1)	2.753 (3)	2.740 (3)
(Ni,Fe)–O (x6) (Å)	1.948 (1)	1.955 (1)	1.961 (3)	1.954 (3)
(Ni,Fe)–O–(Ni,Fe) (°)	169.3 (1)	164.8 (1)	164.0 (2)	162.8 (2)
χ^2	1.09	1.08	1.12	

[a] Assuming stoichiometric oxygen content.

electrical conductivity values obtained from the four-probe DC measurements, the porosity of the samples (24, 23 and 28% for the bars with G/N = 0.5, 1.0 and 1.5, respectively) and its effect on the electrical conductivity must be mentioned. The incorporation of pores significantly degrades the electrical characteristics of the material [27]. As has been observed by other authors [26,28], as the porosity in the specimen increases the contact points between the two neighboring grains or interconnectivity between the grains decrease and this results in a decrease in the conductivity of the specimen.

As can be observed, at the same calcination temperature, the material obtained with G/N = 1.0 shows the higher specific conductivity. Therefore the preparation route has an important influence on the electrical properties of the obtained materials. This result consisted of the morphological analysis previously reported which indicates that this material ($LaNi_{0.6}Fe_{0.4}O_3$; G/N = 1.0) seems to be better sintered. Table 3 lists the electrical conductivity obtained for the sintered samples at 600, 700 and 800 °C and the geometrical and relative density calculated for the pellets.

The conductivity values obtained for the present compounds are not directly comparable with the literature conductivity data for $LaNi_{0.6}Fe_{0.4}O_3$ materials [14,24,25,29] because these results are obtained on samples prepared using different chemical routes and/or calcined at different temperatures from ours. Overall, the conductivity values obtained in this work are adequate for the contact layer

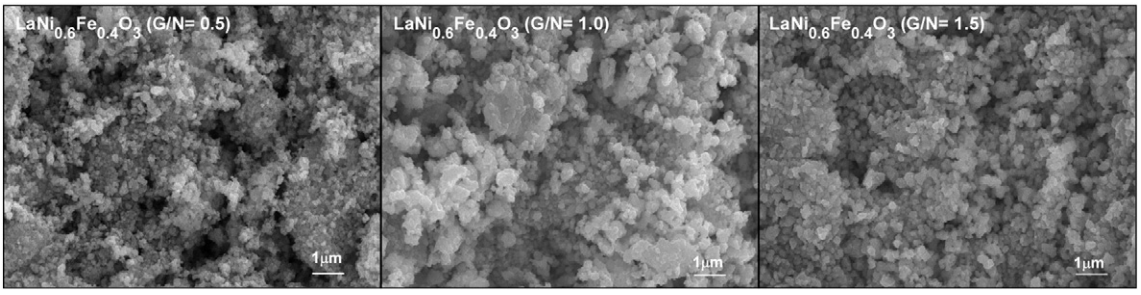

Fig. 3. SEM images for the combustion-synthesized LNF after a sintering treatment at 850 °C, as obtained at different fuel conditions.

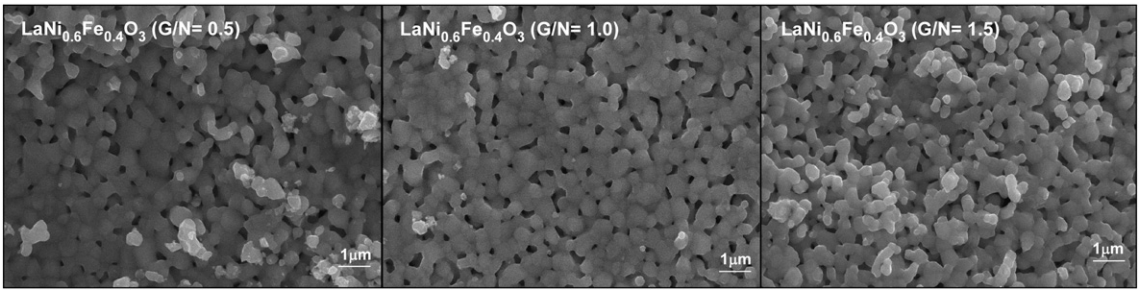

Fig. 4. SEM micrographs taken on the surface of the $LaNi_{0.6}Fe_{0.4}O_3$ pellets sintered at 1050 °C during 5 h.

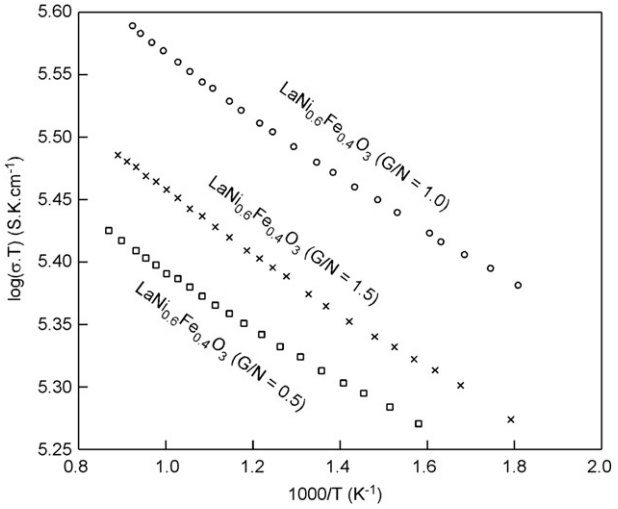

Fig. 5. Arrhenius plot of $LaNi_{0.6}Fe_{0.4}O_3$ perovskites as a function of temperature.

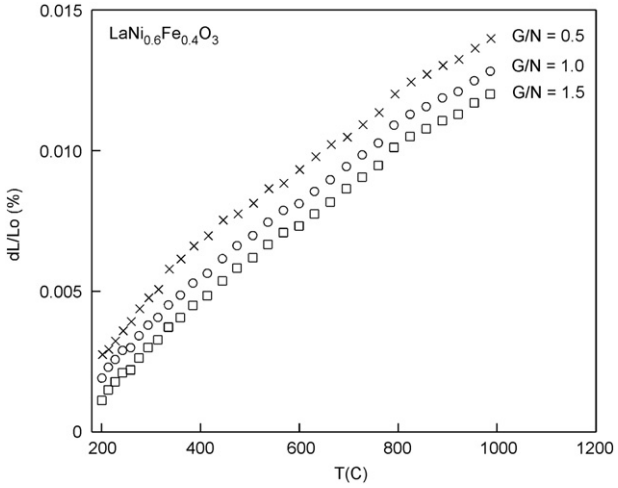

Fig. 6. Thermal expansion behavior of $LaNi_{0.6}Fe_{0.4}O_3$ perovskites obtained by the glycine-nitrate route using different amounts of fuel/oxidizer ratio (G / N = 0.5, 1.0 and 1.5).

application in IT-SOFCs, despite having low values of density (see Table 3).

The activation energy obtained from the Arrhenius plots for all compounds is 0.02 eV, in good agreement with the previously reported value [14].

3.4. Thermal expansion study

In order to determine the mechanical compatibility of the three cathode contact materials with the other cell components, thermal expansion measurements on rectangular bars were carried out in air atmosphere. Fig. 6 shows the thermal expansion curves of the samples obtained upon heating from 200 to 1000 °C.

The thermal expansion curves were fitted by two straight lines. The change in slope observed in high temperature range in the thermal expansion behavior is considered to be due to loss of lattice oxygen and the formation of oxygen vacancies [30,31].

The value of the average linear thermal expansion coefficient of the samples is given in Table 3 for the different temperature ranges.

As can be observed, the TEC values increase slightly with an increase in the G/N molar ratio in the temperature range studied, with the most significant change for the G/N = 1.5 sample, which appeared to contain two closely related perovskite phases. Further studies of the variation of density on the properties of the material [25,32], indicate that the obtained density after sintering only has a negligible influence on TEC of the samples. Consequently, it is possible to say that the TEC values obtained match with those of the cathode and interconnect materials [33,34].

Table 3
Electrical conductivity values at different temperatures, activation energy, geometrical and relative density of the pellets, and average TEC values in different temperature ranges for $LaNi_{0.6}Fe_{0.4}O_3$ perovskites prepared using glycine/nitrate molar ratios of 0.5, 1.0 and 1.5.

G/N	0.5	1.0	1.5
$\sigma_{(600\ °C)}$ (S/cm)	362	387	301
$\sigma_{(700\ °C)}$ (S/cm)	250	373	291
$\sigma_{(800\ °C)}$ (S/cm)	239	360	279
Ea (eV)	0.02	0.02	0.02
ρ_{exp} (g·cm^{-3})	5.30	5.34	5.03
ρ_{exp}/ρ_{the}	0.76	0.77	0.72
Average $TEC_{(200-600\ °C)}$ (1.10^{-6} °C^{-1})	15.26	15.81	17.22
Average $TEC_{(600-1000\ °C)}$ (1.10^{-6} °C^{-1})	11.93	12.43	12.52

4. Conclusions

Three $LaNi_{0.6}Fe_{0.4}O_3$ compounds have been obtained by glycine-nitrate method varying the fuel/oxidizer ratio (G/N = 0.5, 1.0 and 1.5) in order to study the effect on the structure, morphological and electrical properties. At room temperature, all compounds have rhombohedral symmetry (S.G.: $R\bar{3}c$). A slight structure change to a less symmetric structure of the perovskite by increasing the fuel/oxidant ratio has been observed. The compound obtained with stoichiometric G/N value presents the most suitable characteristics as a cathode contact material: better sinterability, higher values of electrical conductivity and suitable value of TEC. Therefore, it can be concluded that the glycine-nitrate process, with an optimal G/N ratio of 1.0, is a more appropriate technique for preparing a promising $LaNi_{0.6}Fe_{0.4}O_3$ candidate cathode contact material for IT-SOFC applications.

Acknowledgments

This research has been funded by the Dpto. Educación, Política Lingüística y Cultura of the Basque Goverment (IT-630-13), Ministerio de Economía y Competitividad (MAT2013-42092-R) and the Engineering and Physical Sciences Research Council (EP/I003932). The authors thank SGIker Universidad del País Vasco/ Euskal Herriko Unibertsitatea (UPV/EHU) technical support. K. Vidal thanks UPV/EHU for funding.

References

[1] D. Medvedev, A. Murashkina, E. Pikalova, A. Demin, A. Podias, P. Tsiakaras, Prog. Mater. Sci. 60 (2014) 72–129.
[2] K. Vidal, L.M. Rodríguez-Martínez, L. Ortega-San-Martín, M.L. Nó, T. Rojo, M.I. Arriortua, Fuel Cells 11 (1) (2011) 51–58.
[3] A. Ecija, K. Vidal, A. Larrañaga, L. Ortega-San-Martín, M.I. Arriortua, in: Yitzhak Mastai (Ed.), 2012 [ISBN: 978-953-51-0581-7. Available from: http://www.intechopen.com/books/advances-in-crystallization-processes/synthetic-methods-for-perovskite-materials-structure-and-morphology].
[4] C.R. Milian, T. Mariño, E. Pérez, O.L. Alves, P. Aranda, M. Aguilar, Y. Mosqueda, Ceram. Int. 40 (2014) 249–256.
[5] F. Deganello, G. Marcí, G. Deganello, J. Eur. Ceram. Soc. 29 (2009) 439–450.
[6] A. Kumar, A.S. Mukasyan, E.E. Wolf, Appl. Catal. A Gen. 401 (2011) 20–28.
[7] M.Th. Makhlouf, B.M. Abu-Zied, T.H. Mansoure, Adv. Powder Technol. 25 (2014) 560–566.
[8] C. Zhu, A. Nobuta, I. Nakatsugawa, T. Akiyama, Int. J. Hydrogen. Energ. 38 (2013) 12238–13248.
[9] H. Najjar, J.F. Lamonier, O. Mentré, J.M. Giraudon, H. Batis, Appl. Catal. B Environ. 106 (2011) 149–159.
[10] R.S. Guo, Q.T. Wei, H.L. Li, F.H. Wang, Mater. Lett. 60 (2006) 261–265.
[11] J. Ma, C. Jiang, X. Zhou, G. Meng, X. Liu, J. Power Sources 162 (2) (2006) 1082–1087.
[12] L.D. Jadhav, M.G. Chourashiya, K.M. Subhedar, A.K. Tyagi, J.Y. Patil, J. Alloys Compd. 470 (1–2) (2009) 383–386.
[13] Z. Shao, W. Zhou, Z. Zhu, Prog. Mater. Sci. 57 (2012) 804–874.

[14] A. Morán-Ruiz, K. Vidal, M.A. Laguna-Bercero, A. Larrañaga, M.I. Arriortua, J. Power, Sources 248 (2014) 1067–1076.
[15] F. Wang, D. Yan, W. Zhang, B. Chi, J. Pu, L. Jian, J. Pu, L. Jian, Int. J. Hydrogen. Energ. 38 (2013) 646–651.
[16] Z. Yang, G. Xia, P. Singh, J.W. Stevenson, J. Power, Sources 155 (2006) 246–252.
[17] B.P. McCarthy, L.R. Pederson, Y.S. Chou, X.D. Zhou, W.A. Surdova, L.C. Wilson, J. Power, Sources 180 (2008) 294–300.
[18] A. Morán-Ruiz, K. Vidal, A. Larrañaga, M.I. Arriortua, Fuel Cells 13 (2013) 398–403.
[19] M. Rietveld, J. Appl. Crystallogr. 2 (1969) 65–71.
[20] A.C. Larson, R.B. Von Dreele, GSAS: General Structure Analysis System, LAUR, 1994. 86–748.
[21] J.Y. Chen, J. Rebello, V. Vashook, D.M. Trots, S.R. Wan, T.L. Wen, J. Zosel, U. Guth, Solid State Ionics 192 (2011) 424–430.
[22] R.N. Basu, F. Tietz, O. Teller, E. Wessel, H.P. Buchkremer, D. Stöver, J. Solid State Electrochem. 7 (2003) 416–420.
[23] N. Sukpirom, S. Iamsaard, S. Charojrochkul, J. Yenyongchaiwat, J. Mater. Sci. 46 (2011) 6500–6507.
[24] M. Bevilacqua, T. Montini, C. Tavagnacco, G. Vicario, P. Fornasiero, M. Graziani, Solid State Ionics 177 (2006) 2957–2965.
[25] E. Niwa, C. Uematsu, T. Hashimoto, Mater. Res. Bull. 48 (2013) 1–6.
[26] R. Chiba, F. Yoshimura, Y. Sakurai, Solid State Ionics 124 (1999) 281–288.
[27] K.Y. Yiang, W.J. Yoo, A. Krishnamoorthy, IEEE Trans. Electr. Devices 52 (2005) 490–494.
[28] M.B. Kakade, S. Ramanathan, D. Das, Cera. Int. 37 (2011) 195–200.
[29] R.N. Basu, F. Tietz, E. Wessel, H.P. Buchkremer, D. Stöver, Mater. Res. Bull. 39 (2004) 1335–1345.
[30] C. Nityanand, W.B. Nalin, B.S. Rajkumar, C.M. Chandra, Solid State Ionics 13 (2011) 1022–1030.
[31] X. Ding, X. Kong, J. Jiang, C. Cui, X. Guo, Mater. Res. Bull. 45 (2010) 1271–1277.
[32] S. Wang, B. Lin, K. Xie, Y. Dong, X. Liu, G. Meng, J. Alloy. Compd. 468 (2009) 499–504.
[33] J. Piron Abellan, V. Shemet, F. Tietz, L. Singheiser, W.J. Quadakkers, in: H. Yokokawa, S.C. Singhal (Eds.), Proceedings of the 7th International Symposium on Solid Oxide Fuel Cells (SOFC VII), The Electrochemical Society Proceedings, Pennington, NJ, 2001, p. 811 [PV. 2001–16].
[34] C. Sun, R. Hui, J. Roller, J. Solid State Electrochem. 14 (2010) 1125–1144.